Comparison of RANS and LES in high pressure turbines

R. Fransen [a], E. Collado Morata [a], F. Duchaine [b], N. Gourdain [b], L.Y.M. Gicquel [b], L. Vial [a], G. Bonneau [a],

[a] *Safran Turbomeca, DT/MD/MO, 64511 Bordes Cedex 1, France*
[b] *CERFACS, 42 Av. G. Coriolis, 31057 Toulouse, France*

Received *****; accepted after revision +++++

Presented by

Abstract

Future combustors can greatly benefit from advanced coupled simulations directly inheriting from the experience and deployment of massively parallel tools dedicated to the predictions of flows in the combustor and in the turbine. While LES is widely used for combustion chambers, its application to turbine flows is only beginning. In that respect, being able to couple or simply simulate in an integrated form the combustion chamber and the turbine is the key to control the maximum temperature reached on the turbine blades and therefore the performances of the engine. In a first attempt towards this objective, the application of a LES solver coming from the combustion community (AVBP) to two typical turbine cases is compared to RANS predictions obtained with a code specifically built for turbine flows (elsA). The first application is an inlet guide vane which operates at high subsonic Mach and Reynolds numbers, close to operating conditions of an industrial configuration. The comparison of LES results with experimental data indicates that LES is able to correctly predict the aerodynamics and its impact on the heat transfer, while RANS fail in predicting the wall heat transfer (for a high inlet turbulence intensity). The second application is an academic case representative of an internal cooling channel of a high pressure turbine blade: aerodynamics and thermal properties have been extracted from LES as well as RANS and compared to measurements performed in a rib-roughened channel with a high-blockage ratio. Results show that if RANS do not reproduce correctly the flow and associated thermal effect near the wall, LES gives very good predictions of fluid motion and mixing leading to improved wall temperature evaluations.

Résumé

Comparaisons RANS et LES dans les turbines haute pression

Le développement des prochaines chambres de combustion peut fortement bénéficier des méthodes avancées de simulations couplées grâce à l'expérience acquise et au large déploiement d'outils massivement parallèles pour la prédiction des écoulements dans la chambre de combustion et la turbine. Alors que la LES est déjà largement utilisée pour les calculs de chambre de combustion, son application pour les écoulements dans les turbines n'en est qu'à ses débuts. Dans ce contexte, être capable de coupler ou de simplement simuler sous la forme d'un seul ensemble la chambre et la turbine est la clé pour controler la température maximale atteinte sur les aubes de turbines et ainsi les performances du moteur. Dans une première tentative en vue de cet objectif, l'application d'un solveur LES provenant de la communauté combustion (AVBP) à deux configurations typiques de turbine est comparée aux prédictions RANS obtenues avec un code spécifiquement dédié pour les écoulements dans les turbines (elsA). La première application est un diffuseur opérant à Mach subsonique élevé et haut nombre de Reynolds, proche des conditions opératoires d'une configuration industrielle. La comparaison des résultats LES avec les données expérimentales montre que la LES est capable de prédire correctement l'aérodynamique ainsi que son impact sur les transferts

de chaleur, tandis que le RANS donne des prédictions des transferts thermiques aux parois de moindre qualité. La seconde application est un cas académique représentatif d'un canal de refroidissement interne d'une aube de turbine haute pression. Les comparaisons RANS et LES avec des mesures expérimentales montrent que si le RANS ne parvient pas à reproduire correctement l'écoulement et les effets thermiques associés près des parois, la LES donne en revanche une très bonne prédiction de la structure du fluide conduisant ainsi à une meilleure évaluation de la température aux parois.

Key words: Large Eddy Simulation ; Gas Turbine ; Heat Transfer

1. Introduction

Modern gas turbine especially designed to be more and more efficient rely on a consequent increase of the inlet temparature of the combustion chamber, thereby increasing the chamber outlet temperature. Accurate predictions of these inlet turbine values become really necessary to ensure a more precise estimate of turbine lifetime. Thanks to increasing computer power, new numerical methods become of first interest to compute such complex configurations: the numerical models that have already shown their benefit for designing flame tubes and combustors can now be used in coupled simulations to compute both the fluid and the solid thermal evolutions in the turbine. The second advantage for using the same models for all the parts of the gas turbine is the possibilty to finally simulate the whole engine in one simulation.
LES model is one of these new tools that allow to progress significantly by alleviating turbulence modeling efforts. In order to qualify this model for better heat transfer predictions, this article provides two test cases representative of gas turbine applications for which LES and RANS models are currently used in industrial gas turbine design processes. The first section presents the governing equations of the RANS and LES models and the two codes used for these applications. In a second part, the flow around a blade is studied followed by cooling passages designed inside the blade.

2. Modelisation and tools

The high Reynolds numbers related to the present studies are too computationally expensive to be simulate them directly with DNS in the context of practical engineering calculations, as on Fig. 1. Instead, the instantaneous (exact) governing equations can be time-averaged, ensemble-averaged, or otherwise manipulated to remove the small scales, resulting in a modifed set of equations that are computationally less expensive to solve. However, the modified equations contain additional unknown variables and turbulence models are needed to close the system before being simulated numerically. The most common approach for complex configurations is still the Reynolds-Averaged Navier Stokes methods (RANS) that proposes to model the effect of all the turbulent scales on the mean flow.

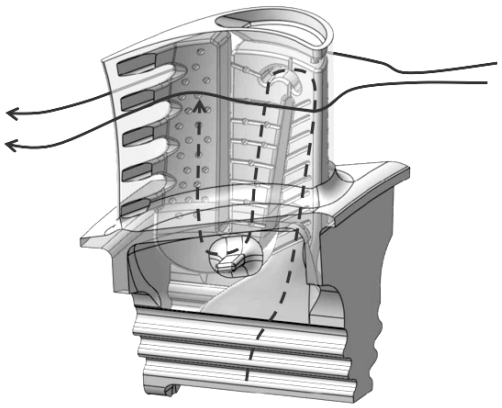

Figure 1. Example of application for the two test cases of this study : flow around (solid arrow) and inside (dashed arrow) a turbine blade.

An alternative and more universal method is the Large-Eddy Simulation (LES) that introduces a separation between the resolved (large) turbulent scales and the modelled (small) scales [16,14,13]. Both RANS and LES methods, detailled below, have been heavily tested on aerodynamic setups and to a lesser extent on thermal problems.

Email addresses: remy.fransen@cerfacs.fr (R. Fransen), elena.collado@cerfacs.fr (E. Collado Morata).

These two configurations are representative of industrial application as shown on Fig. 1 : typical flows around and inside parts of turbine stage are computed. For our work, two flow solvers are considered: a structured multi-block solver (elsA) [21] and an unstructured solver (AVBP) [8,17].

The governing equations for both approaches are the unsteady compressible Navier-Stokes equations that describe the conservation of mass, momentum and energy. In conservative form, it can be expressed in three-dimensional coordinates as:

$$\frac{dW}{dt} + divF = 0 \tag{1}$$

where W is the vector of primary variables, $F = (f - f_v, g - g_v, h - h_v)$ is the flux tensor; f, g, h are the inviscid fluxes and f_v, g_v, h_v are the viscous fluxes. The fluid follows the ideal gas law $p = \rho\, r\, T$, where r is the mixture gas constant. The fluid viscosity follows Sutherland's law and the heat flux follows Fourier's law.

2.1. *RANS approach*

This modeling is one of the most used for engineering work. The principle is based on the Reynolds decomposition of the Navier-Stokes equations, splitting each quantity (velocity and pressure) into a mean and a fluctuating component:

$$F = \overline{F} + f' \text{ where } \overline{f'} = 0 \tag{2}$$

Substituting (2) into the Navier-Stokes equations (1) and averaging one obtains :

$$\frac{\partial \overline{\rho}\overline{U}_i}{\partial x_i} = 0 \tag{3}$$

$$\left(\frac{\partial \overline{\rho}\overline{U}_i}{\partial t} + \frac{\partial \overline{\rho}\overline{U}_i\overline{U}_j}{\partial x_j}\right) = -\frac{\partial \overline{P}}{\partial x_i} + \mu\frac{\partial^2 \overline{U}_i}{\partial x_j \partial x_j} - \frac{\partial}{\partial x_j}\left(-\overline{\tau_{ij}}\right) \tag{4}$$

The Reynolds averaging introduces a new term $\overline{\tau_{ij}} = -\overline{\rho u_i' u_j'}$ in the equation of momentum, also called the Reynolds stresses. To close the system, it is necessary to model these stresses. A common model employs the Boussinesq hypothesis [18], which results in:

$$\overline{\tau_{ij}} = 2\overline{\rho}\nu_t\overline{S}_{ij} - \frac{2}{3}\overline{\rho}k\delta_{ij} = \overline{\rho}\nu_t\left(\frac{\partial \overline{U}_i}{\partial x_j} + \frac{\partial \overline{U}_j}{\partial x_i} - \frac{2}{3}\frac{\partial \overline{U}_k}{\partial x_k}\delta_{ij}\right) - \overline{\rho}\frac{2}{3}k\delta_{ij} \tag{5}$$

With k the turbulent kinetic energy, and the new scalar ν_t also known as the turbulent viscosity which has to be modeled. There are numerous types of modelling, classified in terms of number of transport equations solved (in addition to the RANS equations) to compute ν_t [26,25,27]. Here the $k - L$ model [28] is used.

2.2. *LES approach*

LES involves the spatial Favre filtering operation that reduces for spatially, temporally invariant and localised filter functions to:

$$\widetilde{f(\mathbf{x}, t)} = \frac{1}{\overline{\rho(\mathbf{x}, t)}}\int_{-\infty}^{+\infty} \rho(\mathbf{x}', t)\, f(\mathbf{x}', t)\, G(\mathbf{x}' - \mathbf{x})\, d\mathbf{x}', \tag{6}$$

where G denotes the filter function. The unresolved SGS stress tensor $\overline{\tau_{ij}}^t$ is modelled using the Boussinesq assumption [18]:

$$\overline{\tau_{ij}}^t - \frac{1}{3}\,\overline{\tau_{kk}}^t\,\delta_{ij} = -2\,\overline{\rho}\,\nu_t\,\widetilde{S}_{ij}\,, \tag{7}$$

$$\text{with } \widetilde{S}_{ij} = \frac{1}{2}\left(\frac{\partial \widetilde{u}_i}{\partial x_j} + \frac{\partial \widetilde{u}_j}{\partial x_i}\right) - \frac{1}{3}\,\frac{\partial \widetilde{u}_k}{\partial x_k}\,\delta_{ij}. \tag{8}$$

In Eq. (7), $\widetilde{S}_{ij}$ is the resolved strain rate tensor and ν_t is the SGS turbulent viscosity, computed in our case with the WALE model [10], especially designed for wall bounded flow :

$$s_{ij}^d = \frac{1}{2}(\tilde{g}_{ij}^2 + \tilde{g}_{ji}^2) - \frac{1}{3}\tilde{g}_{kk}^2\delta_{ij}, \tag{9}$$

$$\nu_t = (C_w\Delta)^2\frac{(s_{ij}^d s_{ij}^d)^{3/2}}{(\tilde{S}_{ij}\tilde{S}_{ij})^{5/2} + (s_{ij}^d s_{ij}^d)^{5/4}}, \tag{10}$$

In Eq. (10), Δ stands for the filter length ($\propto$ the cubic-root of the cell volume), C_w is the model constant equal to 0.4929 and $\tilde{g}_{ij}$ is the resolved velocity gradient. The SGS energy flux $\bar{q}_i{}^t$ is modeled using a turbulent heat conductivity obtained from ν_t by $\lambda_t = \bar{\rho}\nu_t C_p/\mathrm{Pr}_t$, where $Pr_t = 0.7$ is a constant turbulent Prandtl number, and the gradient of the Favre filtered temperature coming from the modified filtered state equation $\bar{p}=\bar{\rho}r\tilde{T}$ [9,4,22] :

$$\bar{q}_i^t = -\lambda_t\frac{\partial \tilde{T}}{\partial x_i} \tag{11}$$

2.3. *Structured RANS solver*

The *elsA* software uses a cell centered approach on structured multiblock meshes. More information about this flow solver can be found in [21]. Convective fluxes are computed with a second order centered scheme with classical artificial dissipation parameters k^2 and k^4 [6]. Diffusive fluxes are computed with a second-order centered scheme. The pseudo time-marching is performed by using an efficient implicit time integration scheme, based on the backward Euler scheme and a scalar Lower-Upper (LU) Symmetric Successive Over-Relaxation (SSOR) method as proposed in [23]. The turbulent viscosity is computed with the two equations model of [28] based on a $k - L$ formulation and transition is detected with the criterion proposed by [20].

2.4. *Unstructured LES solver*

The parallel LES code, AVBP [8,17], solves the full compressible Navier-Stokes equations using a finite element schemes TTG4A and TTGC based on a two step Taylor Galerkin formulation with a cell-vertex diffusion scheme [7] which is especially designed LES on hybrid meshes. Indeed, low diffusion and low dispersion properties of these explicit schemes are suitable for LES applications and provides 3^{rd} order space and time accuracy. The major drawback of employing explicit schemes is that time steps are very low because CFL number must be below 1 to ensure stability. Therefore, for aerodynamical applications, where the viscous sub-layer needs to be computed, mesh refinements force small time-steps ($\propto 10^{-7}$s) and a higher computational cost.

3. Computational test cases

The two configurations representative of flow around a turbine blade are presented in the following section. Their numerical setup is provided with meshes and boundary conditions details.

3.1. *The LS89 case*

The experimental facility is the isentropic light piston compression tube located at the Von Karman Institute. The tested configuration is a $2D$ turbine blade cascade (the LS 89 blade) largely described in Arts et al. [1]. The vane is mounted in a linear cascade made of five profiles; only the central passage is investigated to correspond to periodic flow conditions. The blade chord C is 67.647 mm with a pitch/chord ratio of 0.85. Experimental investigations are done to measure the blade velocity distribution by means of static pressure tappings and convective heat transfer by means of platinum thin films. Uncertainties are quantified for these measurements and are reported as 0.5% in pressure and 5% on heat transfer rate.

The measurement technique to obtain wall heat fluxes, q_{wall}, is based on information provided by thin film gauges painted on the cascade central blade. The convective heat transfer coefficient, H, is then defined as the ratio between the wall heat flux and the difference between the total free stream, temperature T_0 and the local wall temperature, T_{wall}, Eq. (12).

$$H = \frac{q_{wall}}{T_0 - T_{wall}} \tag{12}$$

A large range of free stream conditions have been experimentally investigated but only two configurations are explored in this work, Table. 1: test cases MUR129 and MUR235, where the subindexes 0 and 2 denote the inlet and outlet flow values, respectively. The considered Reynolds numbers, Re_2, based on the chord and outlet velocity is approximately equal to $1\ 10^6$ for both cases while the inlet Free-Stream Turbulence (FST) intensity, Tu_0, equals 1% or 6% respectively. The last case is representative of the conditions present in a real turbine ($Re \approx 1\ 10^6$ and $Tu_0 \approx 10\%$). Both cases have approximately the same inlet total pressure, $P_{i,0}$ and static mean wall temperature, $T_{s,wall}$.

Test case	Re_2	$M_{is,2}$	$P_{i,0}$	$T_{s,wall}$	Tu_0
MUR129	$1.13\ 10^6$	0.840	$1.87\ 10^5$ Pa	298 K	1.0%
MUR235	$1.15\ 10^6$	0.927	$1.85\ 10^5$ Pa	301 K	6.0%

Table 1
Test cases and details of the flow conditions for VKI experiment.

3.1.1. *Computational domain and mesh generation*

The configuration examined is sketched in Fig 2(a). For RANS, the flow domain is discretized with a multi-block approach, using an O-4H meshing strategy for the guide vane passage (not shown here). The minimum cell size is set to be less than 2 μm all around the blade (corresponding to a mean wall distance y^+ of 1) with an expansion ratio near the wall close to 1.05. Typical grid dimensions are 781 points around the blade and 175 points in the pitchwise direction. Experiments indicate that the mean flow is 2D so the number of points in the spanwise direction being not a critical parameter for RANS, it can be reduced to only 5 points, Table 2(a). Based on this meshing strategy, the blade passage is represented with 0.7×10^6 grid points for RANS.

For the LES unstructured simulations, a hybrid approach with prismatic layers at the wall and tetrahedra in the main duct, Fig. 2(b), is adopted to reduce the number of cells in the nearby region of the wall and to meet the preferential directions of the boundary layer flow. The solution adopted has 5 layers of prisms where the vertical length of the prism Δy is smaller than the triangle base-length Δx. A global consequence is that the minimum cell volume is increased in comparison to a full tetrahedral option. A limit is imposed to this mesh adaptation to avoid numerical errors in these layers, the aspect ratio of the first and thinnest layer is set to $\Delta x^+ \sim \Delta z^+ \sim 4\Delta y^+$, i.e., $x^+ \approx z^+ \approx 4y^+$. The last constraint to control which is critical numerically, is the stretching ratio, 1.09 here. Taking into account all the constraints of this strategy, 29.3×10^6 (6.3×10^6 prisms and 23×10^6 tetrahedra) cells

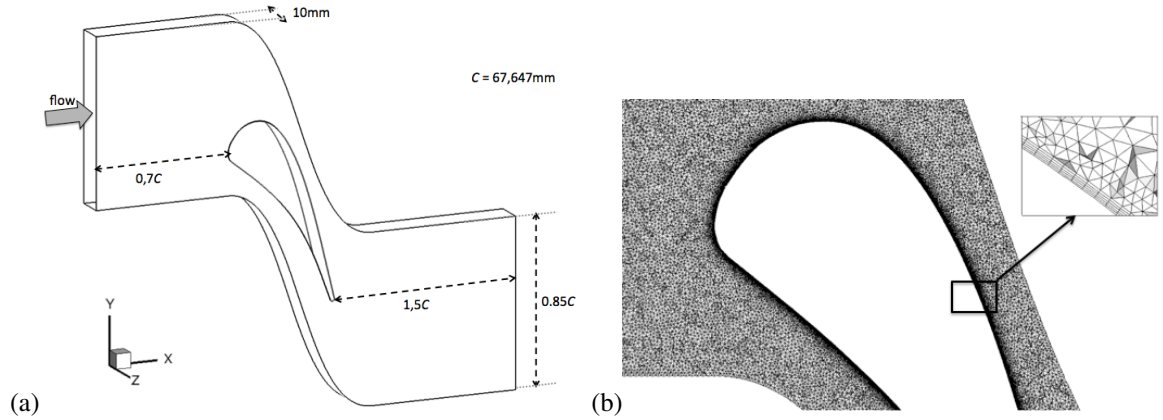

Figure 2. Sketch of the computational domain and unstructured mesh grid.

are required, Table 2(b). Typical grid properties are $6,000$ points around the blade, 200 points in the pitch-wise direction and 230 points in the span-wise direction.

(a)	**RANS**	**LES**
	structured	unstructured
$< y^+ >$	$\sim$1	$\sim$4
1^{st} **layer size**	2μm	8μm
Mesh size	0.7M cells	29.3M cells

(b)	**RANS**	**LES**
	structured	unstructured
CFL	20	0.9
Time-step	1.2 10^{-7}s	1.54 10^{-8}s
CPU cost	t_{RANS}	$\sim 7000\, t_{RANS}$

Table 2
(a) Wall refinement and mesh size for RANS and LES approaches for MUR235 and (b) Temporal parameters and CPU cost comparison for both approaches at MUR235.

The main outcome of such different computational models in agreement with expectations is that LES is much more costly compared to RANS. The main reason is the mesh requirements: up to 30 millions points for LES and only 1 million for RANS. All numerical simulations are performed on a SGI Altix computing platform hosted by the CINES (GENCI). Consequently, RANS only costs 20 CPU hours to reach convergence, Table 2(b), while the equivalent cost with the fully unstructured approach yields to $140,000$ CPU hours (for 10 through-flows times).

3.1.2. *Boundary conditions*

For RANS, an injection condition (turbulence level) is applied at the inlet with parameters based on experimental data, Table. 1, and static pressure is applied downstream to set the outlet isentropic Mach number. An isothermal wall condition is applied at the blade walls with a uniform temperature, T_w=301.15K, as obtained from the experiment. A condition of periodicity is used for lateral and radial sections for both RANS and LES. To take into account the inlet turbulence intensity, the data is given as an input for the RANS simulation. However, this method lacks of adaptability since the value of the turbulence intensity outside the boundary layer must be known, which is not always the case.

For the LES approach, at the inlet of the domain, total temperature and total pressure are enforced using Navier-Stokes Characteristic Boundary Conditions (NSCBC) [12]. At the outlet boundaries, static pressure is imposed using the characteristic NCSBC form. To study the influence of the turbulence intensity on aerothermal quantities, the flow solver shall generate a synthetic turbulent field at the inlet of the domain to mimic the variability of the turbulence levels found in the experimental set-up. The method implemented on the LES unstructured solver was proposed for turbulent boundary conditions by Smirnov [19]. The fluctuating velocity field is obtained from

a sample of random Fourier harmonics. Once the three-dimensional Fourier transform $\hat{\underline{u}}(\underline{k}, t)$ of the fluctuating velocity field $\underline{u_i}'$ of a turbulent flow is done, a spatio-temporal signal is added to the mean boundary flow using Taylor's hypothesis [5]. Note that this generated field does not satisfy the Navier Stokes equations; it only satisfies the continuity equation, so that no noise is produced at the inlet. The last parameter to be chosen is most energetic scale λ_e. It controls the size of the large eddies and therefore, the mesh density to be applied at the inlet if the structures are not to be dissipated by numercis. For a Passot-Pouquet spectrum, the relation between λ_e and the proper length scale of the eddies in the flow, Λ_f, is given by $\Lambda_f \approx 0.4\lambda_e$.

3.2. *Rib-roughened cooling channel case*

The channel of interest (Fig. 3) is a square duct with an hydraulic diameter $D_h = 0.1m$ and aspect ratio of 1 for which experimental measurements have also been carried out at the Von Karman Institute. On one wall, square ribs perpendicular to the flow are mounted with a pitch-to-height ratio (p/h) of 10 leading to a high-blockage ratio, $h/D_h = 0.3$, h being the rib height. The Reynolds number of the mean flow, representative of flows inside real cooling channels, is based on the bulk velocity and D_h and equals 40 000. Aerodynamic flow measurements have been performed using Particle Image Velocimetry (PIV) by Casarsa [3] and thermal analysis using Liquid Crystal Thermography (LCT) by Çakan [2] ; yielding a set of data containing mean flow velocity and fluctuations in the channel and Enhancement Factor (EF) at the wall characterizing the heat-transfer. This last quantity corresponds to the ratio between the measured Nusselt number and Nu_0, the Nusselt number computed from the Dittus-Boelter correlation for a smooth circular duct, as introduced by McAdams [24] :

$$Nu_0 = 0.023 \cdot Re^{0.8} \cdot Pr^{0.4} \tag{13}$$

3.2.1. *Computational domain and mesh generation*

Experimental data has been measured in a section of the channel where a periodic flow is assumed to be established. In order to reduce computational cost and allow finner mesh in LES, the numerical domain is chosen to be only one section of the channel corresponding to one periodic pattern of the channel geometry, see Fig. 3, and periodic boundary conditions are applied between both flow inlet and outlet sections.

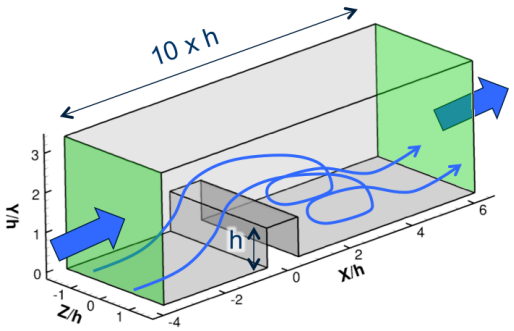

Figure 3. Computational domain

3.2.2. *Boundary conditions*

As said in the previous Section 3.2.1, the domain represents a periodic pattern of the channel for the LES calculation. There is thus no inlet/outlet condition: fluid displacement is obtain adding a source term S_{qdm} similar to a fictive pressure gradient in the momentum equation [11]. S_{qdm} is computed from a mass flow rate target value, such as $S_{qdm} = (\dot{m}_{target} - \dot{m}_{computed})/\tau$.

$$\frac{\partial(\rho u_i)}{\partial t} + \frac{\partial(\rho u_i u_j)}{\partial x_j} = -\frac{\partial p}{\partial x_i} + \frac{\partial \tau_{ij}}{\partial x_j} + S_{qdm} \tag{14}$$

All the others boundaries are walls with adiabatic no-slip condition.

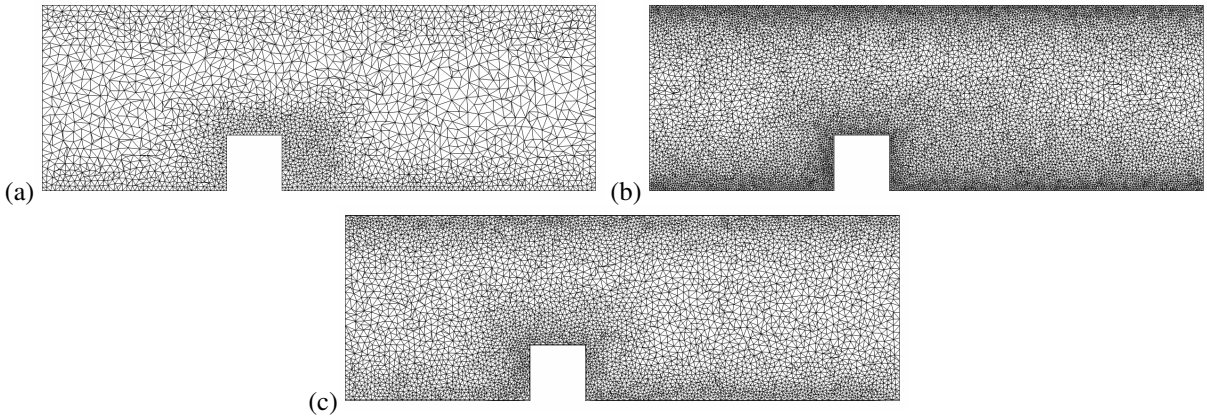

Figure 4. Meshes used for LES: (a) M1, (b) M2 and (c) M3

For LES, three meshes are used to test the influence of the discretization on the results. The first one, called M1, is a coarse full-tetra mesh with low wall resolution but also with a small number of cells allowing bigger computational time step and fast simulations (Fig. 4(a)). The second, M2, is a fine full-tetra mesh with better wall resolution approximately ten times more cells than M1 (Fig. 4(b)). Finally, M3 is an hybrid mesh made of one layer of prisms on all the walls and tetrahedrons everywhere else (Fig. 4(c)). This mesh combines a relative small number of cells with good wall resolution, thanks to the use of prisms at the wall. Characteristics of these three meshes are summarized in the Table 3. As the RANS simulation requests less computation time, no periodic reduction is applied and a full channel with four ribs is discretized with $18.5 \cdot 10^6$ points and a y^+ near 1 on the walls.

Mesh	**Nb. of cells / rib**	y^+	x^+, z^+
M1	550 000	$[5; 20]$	~ 1
M2	5 500 000	$[2.5; 10]$	~ 1
M3	1 800 000	$[1; 5]$	~ 5
RANS	4 500 000	~ 1	~ 40

Table 3
Characteristics of the three meshes used for LES computation of the ribbed channel.

4. Results and Discussions

To qualify the LES solver on the LS89 problem, several computations are produced. RANS and LES results are first compared without FST and then with FST to study the suitability and limits of these approaches if applied in the main veine of the flow within a turbine. These cases are confronted in terms of aerodynamical and thermal predictions. LES Results for ribbed channel are them presented in comparison with PIV and RANS with mean 2D fields. An analysis of turbulence topology is provide to understand where it is created and convected.

4.1. *LS89 case*

A first point of interest of the present investigation is to quantify and qualify the contribution of LES in the context of highly loaded guide vane of turbines. In the following, Figs. 5 & 6, direct qualitative comparisons of the available RANS and LES mean and instantaneous field predictions are produced for the two operating conditions. Global flow features are clearly captured by both approaches: i.e. the blade wake and the flow acceleration on the suction side issued by the profile strong curvature are present in RANS and LES, Fig. 5 (a) & 6 (a). The shock wave is visible in Fig. 6 (b) for the RANS simulation with FST. The well-know Von Karman vortex shedding in the blade's wake is only noticeable in Figs. 6 (a) & (b). Pressure waves emitted from the unsteady boundary layer

detachment at the trailing edge are only present in LES. These pressure waves then travel upstream and downstream the flow interacting with other flow regions.

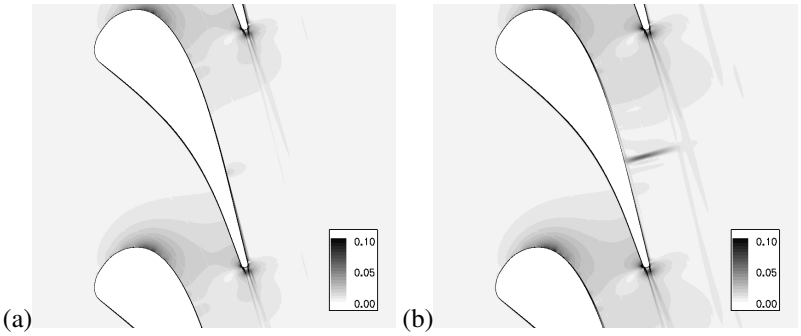

Figure 5. Mean RANS predictions of $||\frac{\partial \rho}{\partial x_i}||/\rho$ for (a) MUR129 and (b) MUR235.

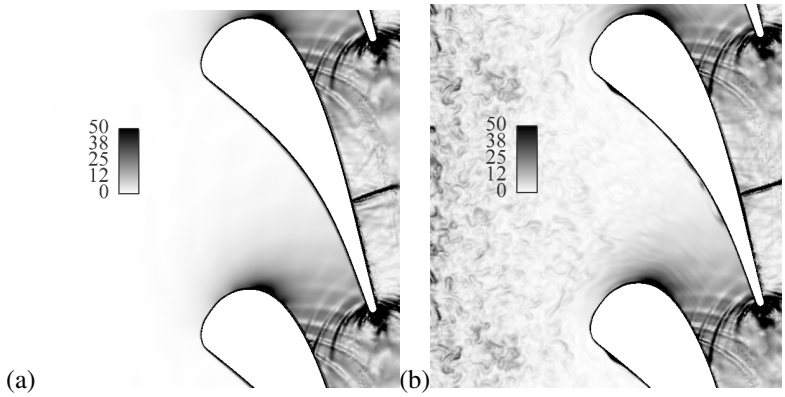

Figure 6. Instantaneous LES predictions of $||\frac{\partial \rho}{\partial x_i}||/\rho$ for (a) MUR129 and (b) MUR235.

An additional difficulty with these conditions is evidenced by the dependency of the flow patterns to the upstream turbulence. When FST exists at the inlet, LES indicates that turbulent flow patterns impact the vane leading edge, leading to the development of vortices on the pressure side which then influence the flow boundary layer along the blade.

Aerodynamic mean field predictions are gauged through the evolution of the isentropic Mach number along the curvilinear abscissa of the blade, S (set equal to zero for the blade leading edge and positive/negative for the pressure side/suction side, respectively). No major distinctions between the two methods are noted for the two cases with and without FST (results are not shown here). A more detailed investigation of the flow boundary layer behavior of the these two predictions is thus carried on looking at the heat transfer flux at the blade wall, Fig. 7.

In the MUR129 test case, Table. 1 and Fig. 7 (a), the boundary layers remain mainly laminar on both suction and pressure sides. The heat transfer coefficient H obtained by RANS and LES is thus correctly estimated on these sides. The common behavior of H for RANS and LES in the near leading edge region corresponds to the development of the laminar boundary layer on both pressure and suction sides. At $S = 62$ mm, corresponding to the shock position, RANS and LES anticipate the boundary layer transition seen on the experimental curve at $S = 68$ mm. This clear difference between numerics and experimental findings is related to the overestimation of the shock strength by both approaches, Fig. 7 (a).

Results of Fig. 7 (b) for the MUR235 case, Table. 1, point to the difficulty for this flow and the impact of the main vane turbulence intensity on the boundary layer behavior. For this specific case and with the model adopted,

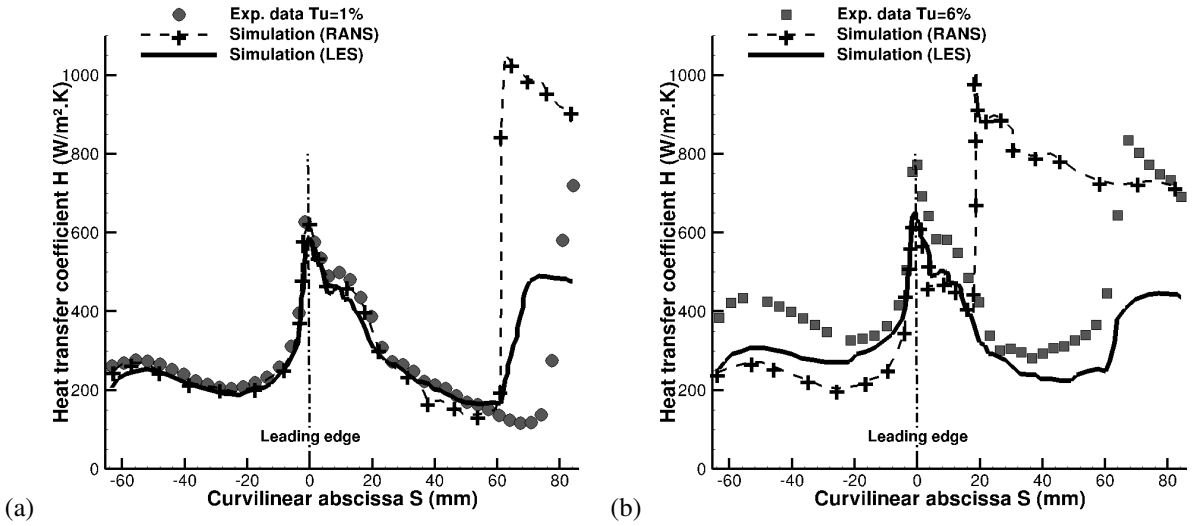

Figure 7. Heat transfer coefficient, H, predicted by RANS and unstructured LES at (a) MUR129 and (b) MUR235.

RANS fails to accurately predict the wall heat transfer. The heat transfer enhancement issued by the main flow turbulence is underestimated by about 30% near the leading edge and the heat transfer coefficient H is identical to the MUR129 test case. On the suction side, RANS locates correctly the onset of transition ($S \approx 20$ mm) but fails in estimating its length leading to a clear overestimation of the heat transfer coefficient at $S = 30$ mm. After $S > 65$ mm, the MUR235 boundary layer is fully turbulent and RANS predicts the correct order of magnitude for the guide vane heating.

LES on the other hand is able to reproduce adequately the boundary layer heat transfer coefficient in the near leading edge region, Fig. 7(b), with an error of 5%. The pressure side development improves if compared to RANS. The heat transfer enhancement is captured by LES but the level of improvement is not sufficient to recover the experimental findings. On the suction side, the LES strategy provides an improvement when compared to RANS especially for the prediction of the location and length of the onset of transition.

The main contribution of LES for this highly loaded blade profile naturally arises from the formalism's ability to reproduce the proper boundary layer transition on the pressure side with increasing FST [15]. Although LES still underestimates the overall heat transfer in the pressure side, the difference with experimental data is reduced to 20% for this approach.

4.2. *Ribbed channel case*

Fig. 8 presents and compares the results in the symmetry plane of the channel for the RANS and two LES (meshes M2 and M3) with respect to the PIV measurement.

Differents phenomena can be analysed in this configuration based on the PIV measurements from Fig. 9. First, when the fluid passes over the rib, its velocity increases because of the section reduction and a maximum is detected in the middle of the channel. A boundary layer separation appears at the upstream rib top corner coinciding with a small flattened recirculation bubble on the top surface of the rib (Fig. 9(1)). Then, just after the rib, since the section suddenly widdens, a second large flow separation occurs at the rib downstream top corner, as encountered in a backward facing step flow. An elongated recirculation bubble takes place behind the rib (Fig. 9(2)), with an associated smaller counter-rotating vortice at the rib downstream bottom corner (Fig. 9(3)), until the flow fully re-expands in the channel and reattach on the bottom wall near $x/h = 4.5$. Finally, when the fluid reaches the next rib, flow streamlines strongly curve upward, leading to a new small recirculation bubble near the upstream bottom

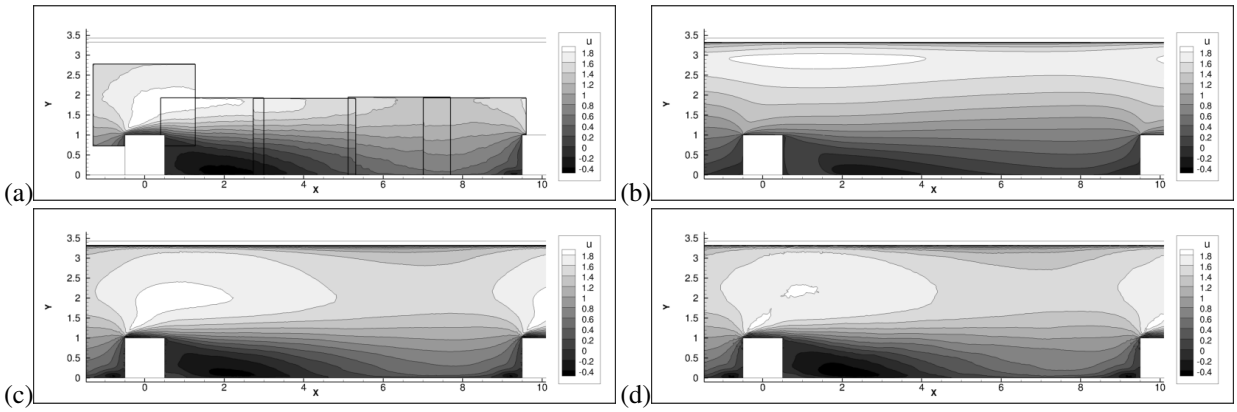

Figure 8. Comparison of the non dimensionalized axial velocity in the symmetry plane for (a) PIV, (b) RANS and LES with (c) M2 and (d) M3 meshes.

corner of the rib (Fig. 9(4)).

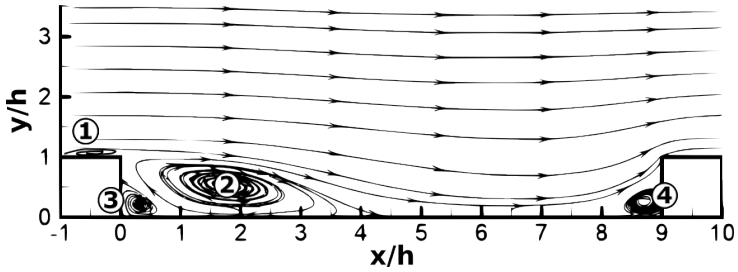

Figure 9. Mean flow topology in the ribbed channel symmetry plane with the four characteristic vortices.

Comparing the numerical simulations with these observations yields important information about the quality of the model used : both LES computations on M2 and M3 mesh (Fig. 8(c)&(d)) show very good agreement with PIV, whereas RANS fail in predicting all the features previously described. Indeed on Fig. 8(b) RANS detects the acceleration near the top wall while LES averages give exactly the good position. Fig. 10 details the comparison at some locations of the middle plane and show the perfect agreement of the LES in the channel, even if some discrepancies may occur in the near-wall region.

Fig. 11 shows the position and the value of turbulent intensity (TI) predicted by LES and measured with PIV. On Fig. 11(a), the maximum of TI has been computed along the channel on one pitch from the upstream top corner of a rib ($x/h = -0.5$) until the next one ($x/h = 9.5$). Comparisons with PIV give very good predictions of both position and size of the zone where most turbulent structures occur and travel. This zone begins in a thin layer at the location of the recirculation bubble Fig. 9(1) above the rib and then spread behind it. The envelope thickness increases from $0.5h$ at position $x/h = 0.5$ to $1.5h$ at $x/h = 4.5$ where the zone reach the bottom wall. After this point, the envelope grows more slightly but stays mainly in the bottom half part of the channel while maximum line keeps a constant position between $y/h = 0.5$ and $y/h = 1.5$.

Fig. 11(b) presents TI detailed values on the maximum line. Reference measurements from PIV detect high turbulence level above the rib between 0.55 and 0.6, then TI decreases until a flat portion between $x/h = 1$ and $x/h = 2.5$ at a mean value of 0.48. These two parts coincide mainly with the location the shear layers of the two vortices Fig 9(1) and Fig 9(2) which maintain the two previous values of intensity. In the second part of the channel where there is no more intense recirculation, TI follows a linear decrease until 0.3 in front of the next rib. LES results give the same evolution of TI but with lower levels. Computations on finer meshes M2 and M3

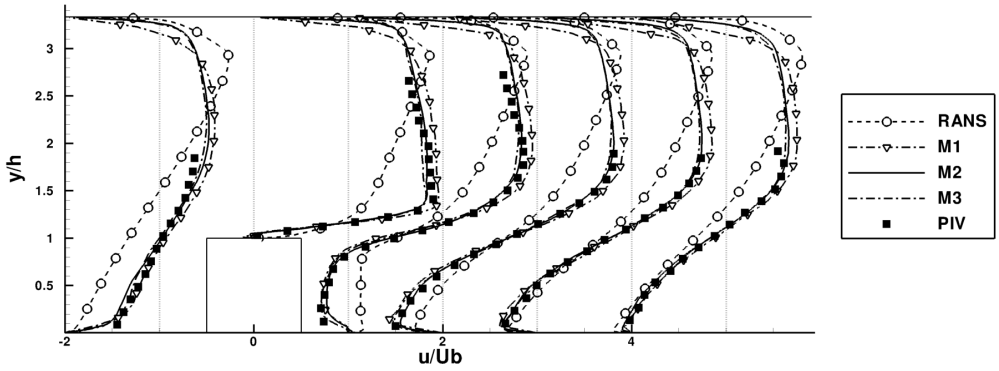

Figure 10. Comparison of LES, RANS and PIV axial mean velocity at different positions in the channel symmetry plane ($x/h = -2, 0, 1, 2, 3, 4$)

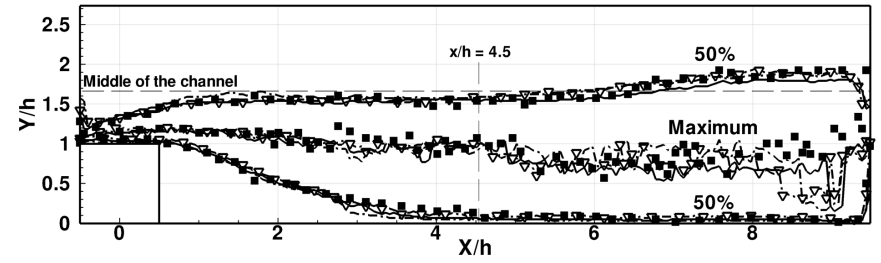

(a)

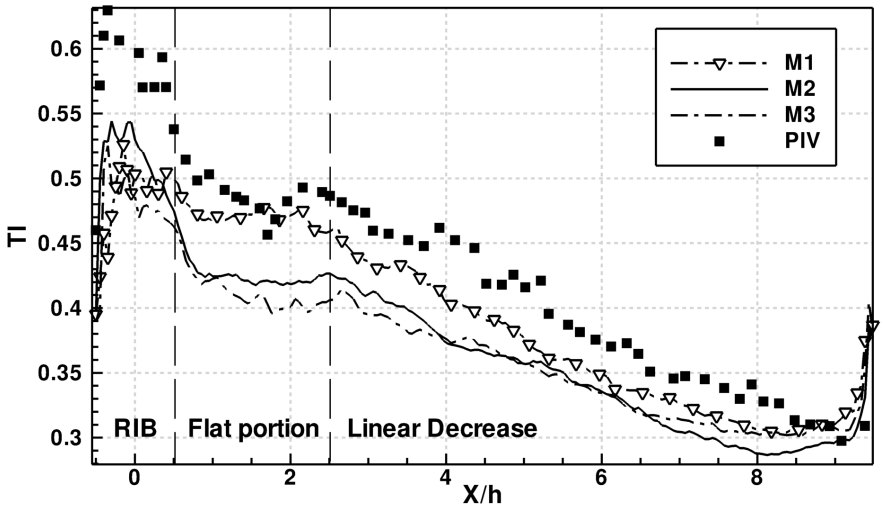

(b)

Figure 11. Comparison of Turbulence Intensity ($TI = \sqrt{\frac{1}{3}(u_{rms}^2 + v_{rms}^2 + w_{rms}^2)}/U_b$) computed with LES: (a) maximum line and envelope (50% of maximum) and (b) value on the maximum line (same legend for both graphs).

reproduce the peak of turbulence above the rib, the lower flat portion and the linear decrease very well while M1 shows a not so contrasted difference between the peak and the flat portion but a good decrease. On the other hand, all values predicted by LES are underestimated against the PIV (around 20% in the peak and flat region and 10% in the linear decrease). Nevertheless, these results do not take into account the subgrid scale contribution for TI, which could reduce the discrepancy between PIV and LES values.

5. Conclusions

This study has been motivated by the need to qualify LES vs RANS for aerodynamic and heat transfer predictions in the complex flows of gas turbines. Two typical configurations have been presented and massively parallel computations with RANS and LES models have been performed. Comparisons with experimental measurements show that:

- LES is more predictive than RANS for this kind of flows. Aerodynamic patterns are better captured by LES impacting on the fluctuations values and heat transfer analysis.
- LES still needs more developments to achieve better predictions on the wall region, i.e., adapted wall law which could reduce the CPU cost and improve the quality of the results.

The benefit of using LES to simulate the high pressure turbine stage is established and would encourage full computations of combustor taking into account the turbine stage to improve predictions of high temperature.

References

[1] T. Arts, M. Lambert de Rouvroit, and A. W. Rutherford. Aero-thermal investigation of a highly loaded transonic turbine guide vane cascade. Technical Note 174, Von Karman Institute for Fluid Dynamics, 1990.

[2] Murat ¸Cakan. *Aero-thermal Investigation of Fixed Rib-roughened Internal Cooling Passages*. PhD thesis, Universit Catholique de Louvain, Von Karman Institute for Fluid Dynamics, 2000.

[3] Luca Casarsa. *Aerodynamic performance investigation of a fixed rib-roughened internal cooling Passage*. PhD thesis, Universita degli Studi di Udine, Von Karman Institute for Fluid Dynamics, 2003.

[4] F. Ducros, P. Comte, and M. Lesieur. Large-eddy simulation of transition to turbulence in a boundary layer developing spatially over a flat plate. *J. Fluid Mech.* , 326:1–36, 1996.

[5] N. Guezennec. *Contrôle actif de la combustion diphasique*. PhD thesis, Institut National Polytechnique de Toulouse, Mars 2010.

[6] A. Jameson, W. Schmidt, and E. Turkel. Numerical solution of the euler equations by finite volume methods using runge-kutta time stepping schemes. In AIAA paper 81-1259, editor, *14th Fluid and Plasma Dynamic Conference*, Palo Alto, 1981.

[7] N. Lamarque. *Schémas numériques et conditions limites pour la simulation aux grandes échelles de la combustion diphasique dans les foyers d'hélicoptère*. Phd thesis, INP Toulouse, 2007.

[8] S. Mendez and F. Nicoud. Large-eddy simulation of a bi-periodic turbulent flow with effusion. *J. Fluid Mech.* , 598:27–65, 2008.

[9] P. Moin, K. D. Squires, W. Cabot, and S. Lee. A dynamic subgrid-scale model for compressible turbulence and scalar transport. *Phys. Fluids* , A 3(11):2746–2757, 1991.

[10] F. Nicoud and F. Ducros. Subgrid-scale stress modelling based on the square of the velocity gradient. *Flow, Turb. and Combustion* , 62(3):183–200, 1999.

[11] S. V. Patankar, C. H. Liu, and E. M. Sparrow. Fully developed flow and heat transfer in ducts having Streamwise-Periodic variations of Cross-Sectional area. *Journal of Heat Transfer*, 99(2):180–186, May 1977.

[12] T. Poinsot and S. Lele. Boundary conditions for direct simulations of compressible viscous flows. *J. Comput. Phys.* , 101(1):104–129, 1992.

[13] T. Poinsot and D. Veynante. *Theoretical and Numerical Combustion*. R.T. Edwards, 2nd edition, 2005.

[14] S. B. Pope. *Turbulent flows*. Cambridge University Press, 2000.

[15] Bhaskaran R. and Lele S. Large eddy simulation of free-stream turbulence effects on heat transfer to a high-pressure turbine cascade. *Journal of Turbulence*, 11(6):1–15, 2010.

[16] P. Sagaut. *Large Eddy Simulation for incompressible flows*. Scientific computation series. Springer-Verlag, 2000.

[17] T. Schønfeld and T. Poinsot. Influence of boundary conditions in LES of premixed combustion instabilities. In *Annual Research Briefs* , pages 73–84. Center for Turbulence Research, NASA Ames/Stanford Univ., 1999.

[18] J. Smagorinsky. General circulation experiments with the primitive equations: 1. the basic experiment. *Mon. Weather Rev.* , 91:99–164, 1963.

[19] A. Smirnov, S. Shi, and I. Celik. Random flow generation technique for large eddy simulations and particle-dynamics modeling. *Trans. ASME. J. Fluids Eng.* , 123:359–371, 2001.

[20] B. Abu-Ghannam and R. Shaw. Natural transition of boundary layers - the effects of turbulence, pressure gradient, and flow history. *J. of Mechanical Engineering Science*, 22(5):213–228, 1980.

[21] L. Cambier and J.P. Veuillot. Status of the elsa cfd software for flow simulationi and multidisciplinary applications. *46th AIAA Aerospace Science Meeting and Exhibit*, (664), 2008.

[22] P. Comte. New tools in turbulence modelling. vortices in incompressible les and non-trivial geometries. Springer-Verlag, France, 1996. Course of Ecole de Physique des Houches.

[23] S. Yoon and A. Jameson. An lu-ssor scheme for the euler and navier-stokes equations. *25th AIAA Aerospace Science Meeting*, 1987.

[24] W.H. McAdams *Heat Transmission*. 2nd edn. McGraw-Hill, New York, 1942.

[25] B. E. Launder, G. J. Reece and W. Rodi. Progress in the Development of a Reynolds-Stress Turbulent Closure. *J. of Fluid Mechanics*, Vol. 68(3), pp. 537-566, 1975.

[26] B.E. Launder and D.B.Spalding. *Lectures in Mathematical Models of Turbulence*. Academic Press, London, England, 1972.

[27] P. R. Spalart, and S. R. Allmaras. A One-Equation Turbulence Model for Aerodynamic Flows. *AIAA Paper*, 92-0439, 1992.

[28] P. R. Spalart, and S. R. Allmaras. Prediction of Hypersonic Shock Wave Turbulent Boundary Layer Interactions With The k-l Two Equaton Turbulence Model. *33rd Aerospace Sciences Meeting and Exhibit*, Reno, NV, Paper No. 95-0232, 1995.